Build Simul (2018) 11: 193–202
https://doi.org/10.1007/s12273-017-0388-6

Air infiltration induced inter-unit dispersion and infectious risk assessment in a high-rise residential building

Yan Wu[1], Jianlei Niu[2] (✉), Xiaoping Liu[3]

1. Department of Building Services Engineering, The Hong Kong Polytechnic University, Hong Kong, China
2. Faculty of Architecture, Design and Planning, The University of Sydney, Australia
3. School of Civil Engineering, HeFei University of Technology, China

Abstract

Identifying possible airborne transmission routes and assessing the associated infectious risks are essential for implementing effective control measures. This study focuses on the infiltration-induced inter-unit pollutant dispersion in a high-rise residential (HRR) building. The outdoor wind pressure distribution on the building facades was obtained from the wind tunnel experiments. And the inter-household infiltration and tracer gas transmission were simulated using multi-zone model. The risk levels along building height and under different wind directions were examined, and influence of component leakage area was analysed. It is found that, the cross-infection risk can be over 20% because of the low air infiltration rate below 0.7 ACH, which is significantly higher than the risk of 9% obtained in our previous on-site measurement with air change rate over 3 ACH. As the air infiltration rate increases along building height, cross-infection risk is generally higher on the lower floors. The effect of wind direction on inter-unit dispersion level is significant, and the presence of a contaminant source in the windward side results in the highest cross-infection risks in other adjacent units on the same floor. Properly improving internal components tightness and increasing air change via external components are beneficial to the control of internal inter-unit transmission induced by infiltration. However, this approach may increase the cross-infection via the external transmission, and effective control measures should be further explored considering multiple transmission routes.

Keywords

air infiltration,
inter-unit dispersion,
infectious risk assessment,
multi-zone modeling,
wind tunnel experiment

Article History

Received: 22 March 2017
Revised: 24 May 2017
Accepted: 5 June 2017

1 Introduction

Airborne transmission is responsible for the spread of various respiratory infectious diseases, such as tuberculosis, measles, influenza, smallpox, and SARS (Riley 1974; Riley et al. 1978; Nicas et al. 2005; Li et al. 2007). Studies after the outbreak of SARS in 2003 attributed the vertical spread of the virus in the re-entrance space of high-rise buildings to the buoyancy-dominant natural ventilation (Yu et al. 2004; Li et al. 2005; Wang et al. 2010a; Cheng et al. 2011). The airborne transmission can trigger a large scale outbreak of an infectious disease due to the rapid spread of pathogens along the airflow (Wu and Niu 2017). Identifying the possible airborne transmission routes related to air movement and assessing the associated infectious risks are essential for implementing effective control measures.

The inter-unit cross-contamination in high-rise residential (HRR) buildings has been a concern as a typical airborne transmission mode ever since the SARS outbreak in 2003 in Hong Kong. Ventilation airflows in HRR buildings involve single-sided ventilation, cross-ventilation and air infiltration. The external transmission induced by the re-entry of single-sided natural ventilation has been comprehensively investigated. Niu and Tung (2008) verified and quantified the vertical upward transmission under buoyancy effects. In such a transmission route, air expelled from the open window of the lower floor re-enters the windows of upper floors. Gao et al. (2008, 2009) and Liu et al. (2010, 2011) further studied the characteristics of inter-unit dispersion induced by single-sided natural ventilation and the cross-contamination

E-mail: jianlei.niu@sydney.edu.au

around a HRR building using CFD modeling approach and wind tunnel experiments. The re-entry ratio can be over 7% and the infectious risk can be 6.6%. Ai and Mak (2014, 2016) systematically evaluated and improved the CFD methods for simulating the single-sided natural ventilation and inter-unit dispersion, especially in predicting of coupled indoor and outdoor airflow and dispersion, and it was found that not only vertically upward, but also vertically downward and horizontal transmission can occur under wind effects along the façade. The effect of mechanical exhausts to prevent inter-unit transmission induced by single-sided natural ventilation was also evaluated (Wu and Niu 2016).

Another internal inter-unit pollutant transmission route driven by air infiltration and cross-ventilation were investigated in our previous on-site measurements (Wu et al. 2016). The measurements were carried out in three horizontal adjacent units on the same floor. The air change rate contributed by thermal effect was estimated in the range of 2%–27% and the mean was 11%. It seems that wind effect is more dominant. The horizontal inter-unit dispersion induced by air infiltration exhibits higher risk than the cross-ventilation because of the low air change rate. The cross-infection risk through this internal air infiltration route assessed using the Wells-Riley Model can reach 9% (Wu et al. 2016), which is higher than the risk of 6.6% via the external vertical spread route through single-sided open windows (Gao et al. 2008). However, the measurements were conducted in an old leaky building with high air infiltration rate over 3 ACH, which may significantly favor the dilution of pathogens and under-estimate the infectious risk. For energy conserving reasons, the recommended value of air leakage in residential buildings is under 0.7–0.8 ACH in the ASHRAE handbook (ASHRAE 2007). The risk assessment of this internal transmission route under lower air infiltration rate should be further studied.

The experimentation is a widely used technique for studying air infiltration, and two common experimental methods are fan pressurization and tracer gas techniques. The former is used to measure the air tightness of the building envelope, while the latter is employed to measure the air infiltration. The multi-zone modeling is another efficient approach that is used in many studies for calculating air infiltration and contaminant transport (Li et al. 2000, 2005; Emmerich 2001; Wang et al. 2010b; Parker et al. 2014). This method simplifies airflow and contaminant-related phenomenon with a few assumptions, which considers each zone as a single node with uniform air conditions. The multi-zone method assumes that the inflow momentum effect in each zone is disregarded. The temperature and contaminant concentration in each zone is supposed to be uniform, and the distribution of pressure is hydrostatic. Air resistance in each zone is neglected while the contaminant transport is considered instantaneously. Given these assumptions, the multi-zone method is unsuitable for describing wind pressure around buildings, and simulating indoor airflow with momentum effects or contaminant gradients. However, it has good performance in solving problems related to entire-building or long-term dynamic simulations and modeling building air infiltrations.

Considering the difficulties to capture the wide range of air-leakage scenarios with measurements, the multi-zone modeling method was used in the present study to reproduce the internal transmission route induced by air infiltration, and to assess the infectious risks under more appropriate air leakage levels. The air infiltration through cracks under wind effect is focused on. The pollutant dispersion characteristics between horizontal adjacent units were examined in a HRR building. The risk levels of cross-infection were assessed along building height and under different wind directions. Moreover, the effects of air airtightness on air infiltration and cross-infection were investigated.

2 Methodology

2.1 Decoupled outdoor wind and indoor infiltration

A major issue in analyzing air infiltration driven by outdoor wind is the accurate solving of the interaction between outdoor wind flow and indoor airflow (Ramponi and Blocken 2012). Figure 1 shows the diagram of the coupled and decoupled approaches. The coupled approach directly solves the outdoor and indoor airflow. While the decoupled approach solves outdoor and indoor flow field separately. The outdoor wind flow is studied first with sealed building assumption and then the indoor airflow is solved based on wind pressure distributions on building façades obtained from the outdoor study.

The coupled approach is difficult to employ when the differences in length scale are substantial or when flow behavior problems exist (Nore et al. 2010). The decoupled approach is simplified compared to the coupled approach, but it is only efficient for certain phenomena. Many studies have verified the applicability of the decoupled approach (Seifert et al. 2006; Kobayashi et al. 2009, 2010). This approach

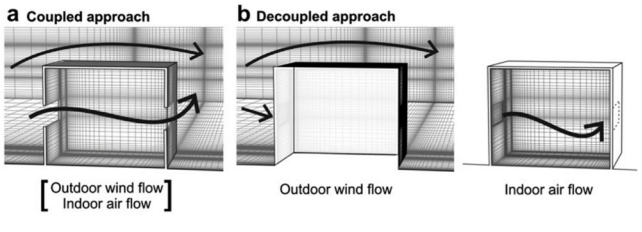

Fig. 1 Diagram of coupled and decoupled approaches (Ramponi and Blocken 2012)

is unsuitable when flow has large openings, specifically when the wall porosities are larger than 10% (Karava et al. 2006, 2007, 2011). And, the approach is impractical when the area of windward openings is significantly smaller than that of the leeward openings (Sandberg 2004). Moreover, the approach cannot be applied when the velocity pressure on the retardation section is larger than the static pressure (Sandberg 2004). In the present study, the decoupled approach is applicable for analyzing air infiltration flow with small cracks and wall porosity. Thus, the decoupled approach was employed.

2.2 Wind tunnel experiment of pressure distributions on building façades

The outdoor airflow patterns around an isolated building and the pressure distributions on building façades were studied using wind tunnel experiments in our previous study (Liu et al. 2010; Liu 2011). The wind tunnel experiments aimed at investigating the cross-contamination around HRR building caused by wind effect. Two sets of experiments were carried out with different building models and wind speeds. In Set 1, a 1:150 scaled 33-story building model without open windows was used, and the experiments were conducted in the high-speed section of the CLP Power Wind/Wave Tunnel in the Hong Kong University of Science and Technology. In Set 2, a 1:30 scaled 10-story building model with open windows was employed, and the experiments were performed in the low-speed section of the wind tunnel. Wind parameters were measured using Gobra Probe. Surface pressures were measured simultaneously by pressure taps (diameter of 0.5 mm), which were connected to 16-channel electronic pressure scanners manufactured by Pressure System Inc. 52 pressure taps were set up in each floor. The incoming wind velocity profile was described using the power law. And the turbulence intensity profile in the wind tunnel test was defined based on the Terrain Category 2 in Australian/New Zealand Standard (Standard 2011), since that the longitudinal turbulence intensity profile at different terrain conditions are only provided in Japan, ECCS 47 (The European Convention for Constructional Steelwork) and Australia. The detailed experiment configuration are introduced in our previous study (Liu 2011). The wind pressure distributions on the high-rise sealed building of Set 1 were utilized as the boundary conditions in the present study for calculating indoor air infiltration in CONTAM. The normalized pressure coefficients on the building envelopes were used to define the pressure conditions of open windows in CONTAM. The experiment configuration and approaching wind profiles of Set 1 is shown in Fig. 2.

2.3 Multi-zone modeling of air infiltration and infectious risk assessment

Indoor air infiltration and inter-unit contaminant transmission were simulated using the multi-zone model, which assumes the uniform distributions of wind pressure, momentum effects, and contaminant concentration in a zone. A multi-zone computer program CONTAM 3.1 was used (Walton and Dols 2003), which has been employed in many research of indoor air quality and contaminant transport (Standard 2011; Temenos et al. 2015; Jomehzadeh et al. 2017). In this program, air infiltration is calculated based on the power law relationship between the flow and pressure difference across a crack in the building envelope as follows:

$$Q = C(\Delta P)^n \quad (1)$$

where Q is the volumetric flow rate (m³/s), ΔP is the pressure drop (Pa), C is the flow coefficient and n is the flow exponent. A variation of the power law equation is related to the orifice

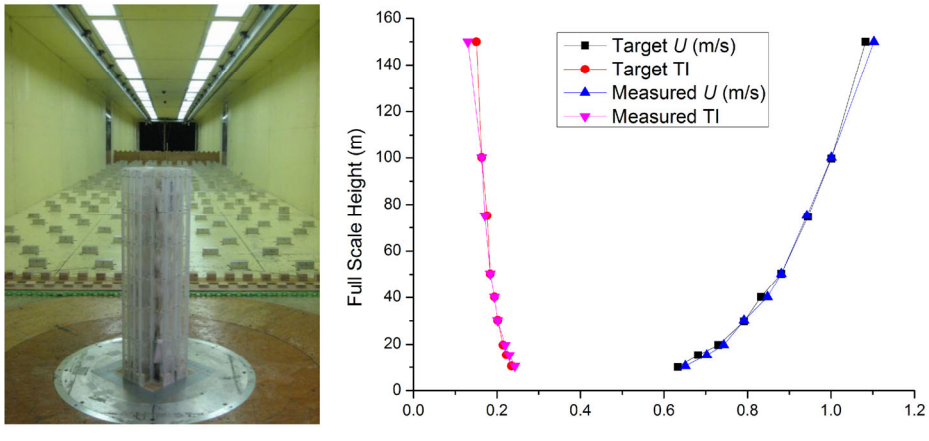

Fig. 2 Configuration of the wind tunnel experiment and approaching wind profiles in our previous study (Liu 2011) (U is the mean velocity, and TI (= u/U) the turbulence intensity, and u is the square root of the mean squared fluctuating velocity. x-axial scales can be used for both U and TI)

equation:

$$Q = C_d A \sqrt{\frac{2\Delta P}{\rho}} \quad (2)$$

where C_d is the discharge coefficient, and A is the component leakage area (m²). The pressure drop and component leakage data are required using this program in calculating the infiltration rate. The pressure data on the building envelopes were obtained from the wind tunnel experiments mentioned above. The leakage areas of components were specified on the basis of the best estimate values in the ASHRAELA Library in CONTAM 3.1 (Walton and Dols 2003).

Infection probability P_i was calculated using the Wells–Riley model to estimate the infectious risk of diseases.

$$P_i = \frac{C}{S} = 1 - e^{\frac{-Iqpt}{Q}} \quad (3)$$

Here, C is the number of infection cases, S is the number of susceptibles. In the calculation, the infector number I in the index unit is 1, the quanta generation rate q is 13 quanta per hour, the pulmonary ventilation rate p of a person is 0.6 m³/h, and the exposure time t is 8 h. The values of the parameters were the same as those in our previous study (Gao et al. 2008; Wu et al. 2016) about the external dispersion for the comparison between two transmission routes. The calculated infectious risks are relative values rather than absolute values. Cross-infection risks for receptor units without a source can be calculated using the following equation:

$$P_i = 1 - e^{\frac{-Iqpt M_i}{Q}} \quad (4)$$

where M_i indicates the mass fraction of air at unit i and originating from source unit (Flat 6).

$$M_i = \frac{c_i}{c_s} \quad (5)$$

where c_i and c_s are the equilibrium tracer gas concentrations of unit i and the source unit (Flat 6), respectively.

2.4 Case settings

To reproduce the horizontal pollutant dispersion induced by air infiltration, a single-floor model (Fig. 3) with nine zones was constructed. The model includes eight units and one lift lobby, which is the same to a typical floor of the cross-type building model in the wind tunnel experiments. The full-scale building was modeled in CONTAM. The vertical transmission via lift shaft or other vertical paths was not included to concentrating on the horizontal route as verified in our previous on-site measurements (Wu et al. 2016). Each unit has three windows that connect the unit to the ambient environment and a door that links the unit to the lift lobby. All windows and doors are closed, but air leakage can easily occur, which are considered as the main airflow paths. A pollutant source is set in Flat 6, which releases tracer gas CO_2 with a constant rate of 500 g/h. CO_2 was used to simulating the diffusion of the gaseous pollutant or fine particles, which exhibit higher pathogenicity than coarse particles. Fine particles less than 1.0 μm disperse similar to gaseous pollutants despite deposition and gravitational effects (Gao et al. 2009). Particles with a size of 0.02–7.00 μm can completely penetrate through building envelopes when the cracks are larger than 1 mm and the pressure difference is higher than 4 Pa (Liu and Nazaroff 2003). However, Tung et al. (1999) experimentally demonstrated that 15%–30% of particles with a size range of 0.43–10.00 μm can be trapped by the building shell. Particle deposition onto indoor surfaces can also limit the spread (Lai and Nazaroff 2000). Therefore, the cross-infectious risk determined using gaseous pollutants may be over-estimated. Besides, considering the low contribution of thermal effect in the airflow and dispersion in our previous on-site measurements (Wu et al. 2016), the thermal effect was neglected in the present study.

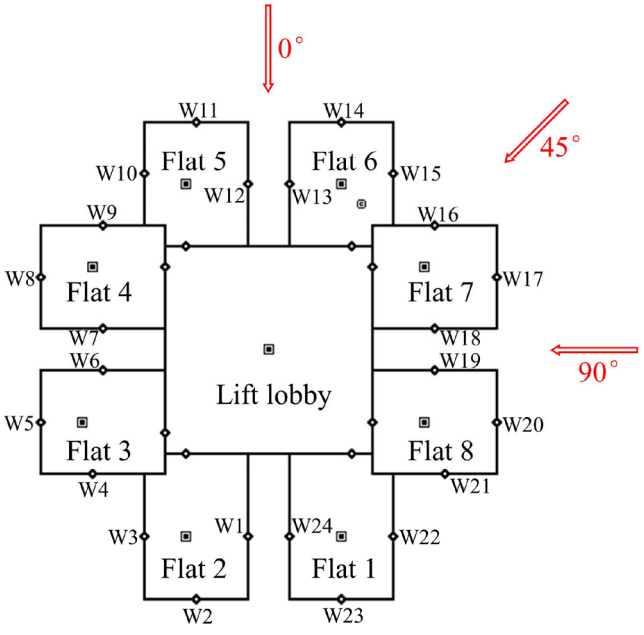

Fig. 3 Schematic diagram of multi-zone model

Four cases on the 4th, 12th, 22nd and 30th floor were calculated to study the characteristics of inter-unit dispersion along building height. Three cases with wind directions of 0°, 45° and 90° were simulated in studying the effect of wind direction. In these cases, the multi-zone models, component leakage data, and tracer gas sources were fixed. The window leakage areas were set to 10 cm²/item and the door leakage area was set to 20 cm²/item. The reference parameters of airflow paths, namely, reference pressure drop and discharge

coefficient C_d, were set to 4 Pa and 1, respectively. Only the pressure boundary conditions were varied for different cases. To study the effects of window or door airtightness on air infiltration and dispersion, 50 cases with different window and door leakage areas were examined. In these cases, all the multi-zone models, tracer gas sources and pressure boundary conditions are fixed, except the window and door leakage data.

3 Results and discussion

3.1 Air infiltration induced dispersion and infectious risk along building height

The wind directions for four different floor cases are all 0°, which means that Flats 4, 5, 6, and 7 are on the windward side and the other units are on the leeward side. The pressure coefficient distributions on building façades of different floors are shown in Fig. 4. The pressure coefficient is defined as:

$$C_P = \frac{(P - P_{ref})}{0.5\rho U_{ref}^2} \quad (6)$$

where P_{ref} is the atmospheric pressure, U_{ref} is the incoming wind velocity at the building height. Similar pressure distribution characteristics on different floors are obtained. The distributions present to be asymmetry. The pressure coefficients on the building façades of the windward side are positive, whereas those on the lateral and leeward sides are negative. High floors generally exhibit large absolute pressure coefficients. However, the pressure coefficients on some façades of the 30th floor are lower than that of the 22nd floor, which can be caused by the separation flow near the roof of the building. Furthermore, the differences in pressure coefficients between various floors are larger on the windward side than those in the leeward side.

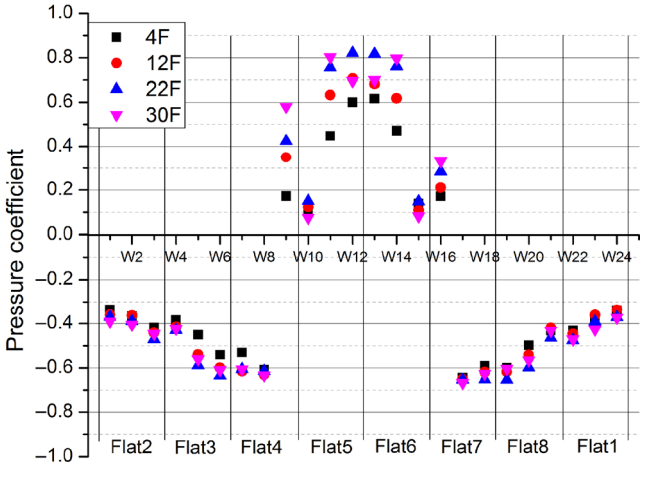

Fig. 4 Pressure coefficients distributions on different floors (wind angle 0°)

Figure 5 compares the infiltration rate of the units on different floors. The air infiltration rate is directly proportional to the pressure difference based on the orifice equation. The infiltration rates of Flats 5 and 6 on the windward side are the largest among the studied units, whereas the infiltration rates of Flats 1 and 2 on the leeward side are the smallest. The infiltration rate reduces gradually from upstream side to downstream side, which can be achieved on all floors. The infiltration rates are nearly symmetrical in the left and right units. This result can be explained by the symmetrical pressure boundary condition. The maximum air infiltration rate is 0.7, which is consistent with the recommended value of air leakage under 0.7–0.8 ACH reported in the ASHRAE handbook.

The air infiltration rate on the windward side significantly increases along building height. And this increase rate slows down along building height. The results of the 22nd and 30th floors are similar. Such similarity may be influenced by the separation flow near the roof. The largest infiltration rates for the lower floor (4th floor), middle floor (12th floor), and higher floors (22nd and 30th floors) are 0.53, 0.62, and 0.69 h^{-1}, respectively. The difference can reach 30%, and the difference in the air infiltration rates of various floors on the leeward side are smaller than that of windward side.

Figure 6 shows the mass fraction of air from Flat 6 to other units, which is used to quantify the internal transmission rate of tracer gas. The mass fractions of air in the leeward units that originate from source unit (Flat 6) are higher than those in the windward units. The mass fractions are below 12% in the windward units and above 35% in the leeward units. The highest mass fraction can reach 50%. This value is significantly higher than 26% in our previous on-site measurements (Wu et al. 2016). The differences in mass fractions among units in the same floor can be more than five times. In the leeward side (Flats 1 and 2), the mass fraction

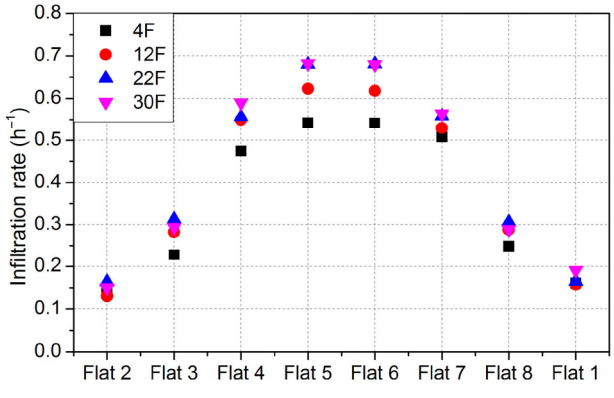

Fig. 5 Air infiltration rate on different floors (wind angle 0°)

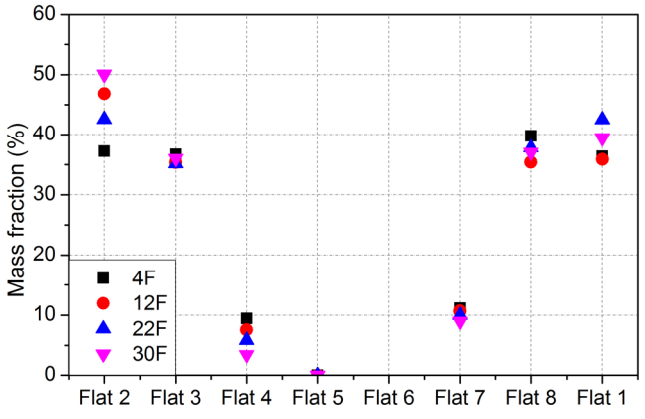

Fig. 6 Mass fractions of air originating from Flat 6 on different floors (wind angle 0°)

elevates along building height. On the contrary, the mass fraction reduces slightly along building height in the lateral and windward side.

The infectious risks on different floors are shown in Fig. 7, which was calculated using the Wells–Riley model. The infectious risk in the index unit is above 40%. In receptor units, leeward units with low air infiltration rates and high mass fractions exhibit high cross-infection probabilities, which are approximately 20%. It is substantially higher than the risks of 9% in the measurements in our previous study (Wu et al. 2016). This result can be attributed to the high air tightness of windows, which dramatically restricts the dilution of pollutants to outdoor space. Lower floor exhibits larger infectious risk than that of higher floor because of the low air infiltration rate, especially in the index and lateral units.

3.2 Air infiltration induced dispersion and infectious risk under different wind directions

Air infiltration and contaminant transmission were calculated under three different wind directions, namely, 0°, 45°, and 90°. The tracer gas sources for all cases are located in Flat 6. The pressure boundary conditions of the 30th floor under three wind directions are extracted from the wind tunnel experiments and presented in Fig. 8. When the wind direction changes clockwise, the maximum value of pressure coefficient also moves clockwise. The windward façades exhibit the highest pressure coefficients, while the leeward and lateral façades show the lowest and middle pressure coefficients, respectively. However, the pressure coefficient distributions are not simply rotate with wind direction because of the non-centro symmetric building configuration in the wind tunnel experiments.

Figure 9 shows the infiltration rate of each unit for cases with various wind directions. Units in the windward side exhibit the maximum infiltration rate in all wind directions. For wind direction of 0°, the infiltration rates in Flats 5 and 6 are the largest among all units. For wind direction 45°, the infiltration rate of Flat 7 is the largest. For wind direction of 90°, the infiltration rate of Flat 8 is the largest. When the

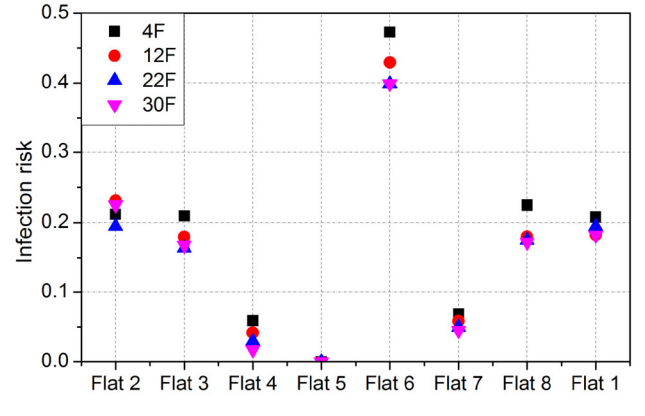

Fig. 7 Infection risks on different floors (wind angle 0°)

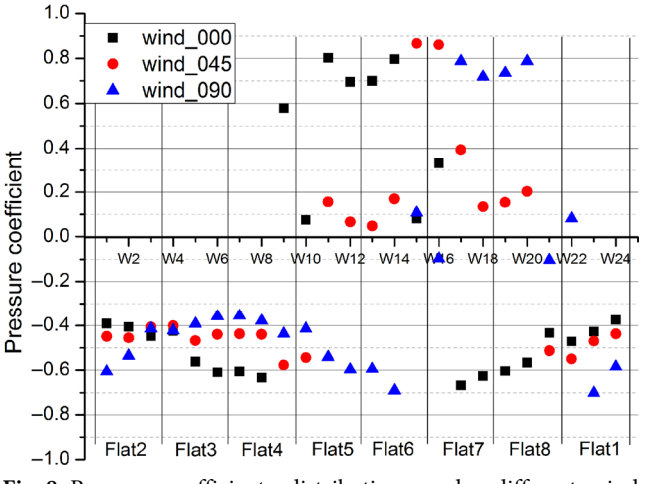

Fig. 8 Pressure coefficients distributions under different wind directions (30th floor)

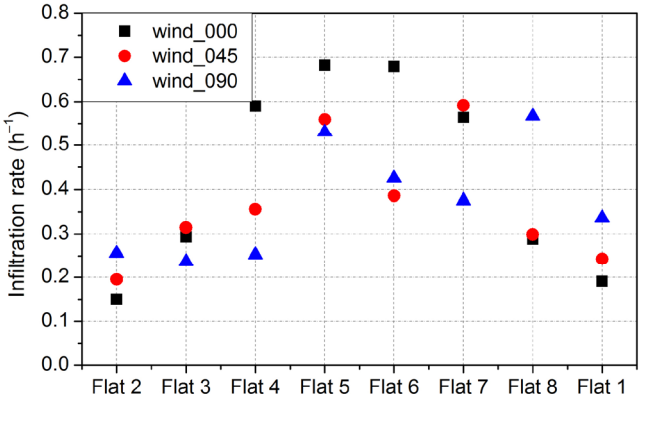

Fig. 9 Infiltration rates in each unit under different wind directions (30th floor)

wind direction changes from 0° to 90°, the maximum infiltration rate decreases slightly. The value is 0.7 for the wind direction of 0°, while 0.6 for the wind directions of 45° and 90°. The air infiltration rates of the leeward units increase when wind direction changes. Accordingly, the difference of infiltration rates among all units decreases.

Figure 10 shows the mass fraction of air in each unit from the source unit under different wind directions. Given the fixed tracer gas source in Flat 6, the effect of wind direction on the exposure levels of other units is significant. When the wind direction is 0°, the maximum mass fraction is 50% in the leeward unit (Flat 2). However, the value is just below 10% when the wind direction changes to 45°. Moreover, tracer gas cannot be detected in other units when the angle of wind direction further increases to 90°. The low mass fractions for the 45° and 90° wind direction cases may be under-estimated because of the limitation that ignoring the re-entry through the outdoor space. Wind direction can significantly affect inter-unit contaminant transmission. The inter-unit dispersion induced by air infiltration suffers most seriously when the contaminant source is in the windward side.

The infectious risks under different wind directions are presented in Fig. 11. When the wind direction is 0° and the index unit is in the windward side, the cross-infection risks in units on the leeward side are high with infectious possibilities near 20%. When the wind direction is 45°, the risks in other horizontal adjacent units are significantly reduced to 5%. Ignoring re-entry through the outdoor space, the cross-infection risk is minimal when the wind direction is 90°. The infectious risk in the index unit is also significantly affected by wind direction. When the index unit is in lateral sides, the infectious risk is significantly higher than that in the windward side. Compared with the effect of different floor in the previous section, the influence of the wind direction is more significant.

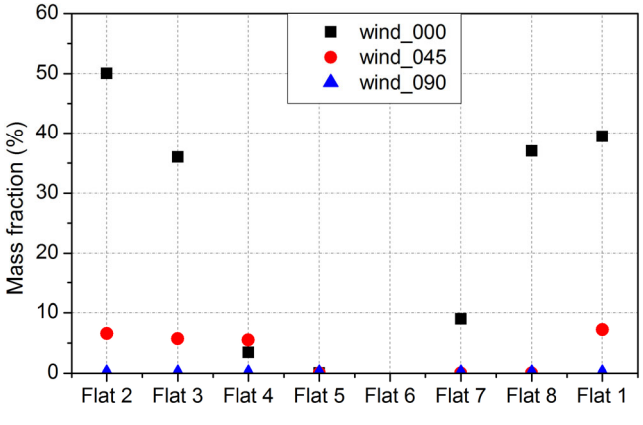

Fig. 10 Mass fraction of air originating from Flat 6 under different wind directions (30th floor)

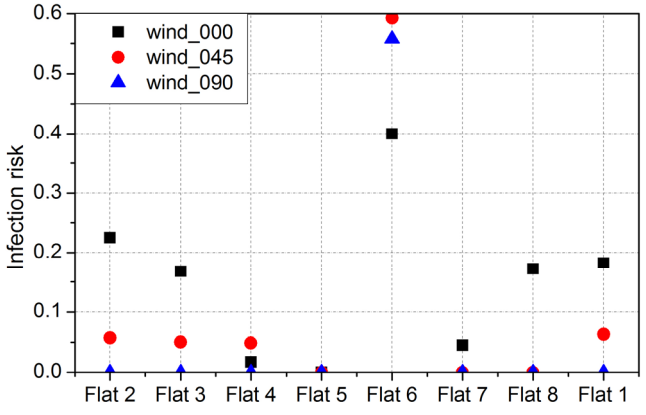

Fig. 11 Infection risks in each unit under different wind directions (30th floor)

3.3 Effect of component air tightness on the cross-infection

To investigate the effect of air tightness on inter-unit pollutant dispersion and cross-infection, cases with different leakage data of windows and doors (representing external airflow path and internal airflow path, respectively) were calculated. The door leakage areas are fixed at 20 cm^2/item in cases with window leakage change. Similarly, the window leakage areas remain at 10 cm^2/item in cases with door leakage change. Figure 12 presents the relationship between leakage area and air infiltration rate. The infiltration rate is proportional to both window and door leakage areas within the scope of the present study. However, the curve of the infiltration rate against window leakage area is significantly steeper. Increasing the window leakage area to 30 cm^2/item or increasing the door leakage area to 80 cm^2/item has the same total leakage area of 110 cm^2, but the infiltration rate of the former case is much higher than that of the latter one. Thus, the effect of window tightness on air infiltration rate is more significant than that of door tightness.

Figure 13 indicates the effects of window or door tightness on indoor contaminant level. For the source unit (Flat 6), both increasing external window and internal door leakage areas can help remove the contaminant. For other receptor units, large external window leakage area can help reduce tracer gas concentration, but large internal door leakage area may lead to high contaminant level. The reason is that large external window leakage area causes advantageous air change with outdoor space. Large internal door leakage area may results in disadvantageous air change with the contaminated lift lobby. But, when the door leakage increases further, the effect may differ. The influence of external window tightness on indoor contaminant level is higher than internal door tightness, which is similar to its effect on air infiltration rate.

The effects of window or door tightness on mass fraction and infectious risk are shown in Fig. 14 and Fig. 15. Enlarging the leakage in the external window reduces the mass fraction, while increasing the leakage in the internal door elevates mass fraction. The effects of window or door tightness on infectious risk are exactly the same as that on tracer gas concentration. Cross-infection risk can be significantly reduced by increasing the leakage of external window. Enlarging door leakage can increase cross-infection risk. And, while the air tightness is better, its effects on cross-infection risk is higher.

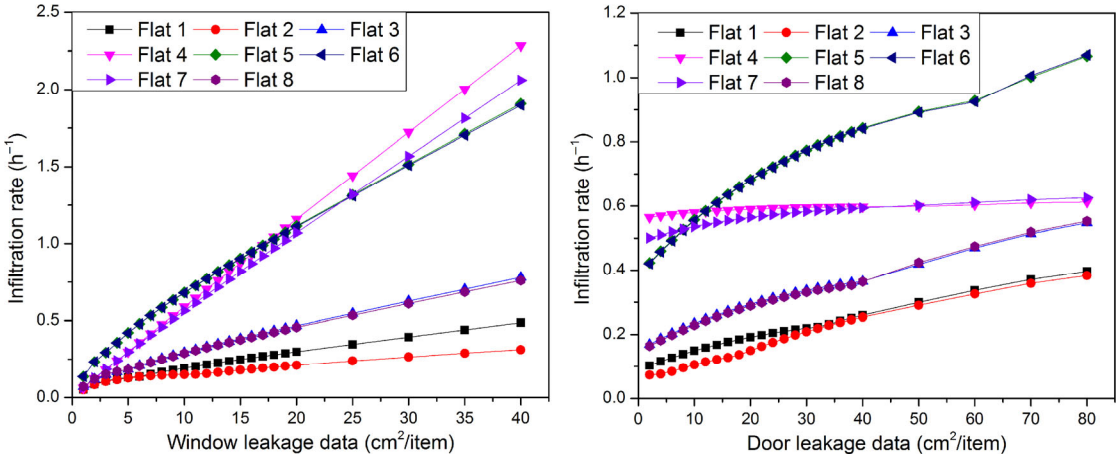

Fig. 12 Effects of air tightness on infiltration rate (Left: window leakage change situation, Right: door leakage change situation)

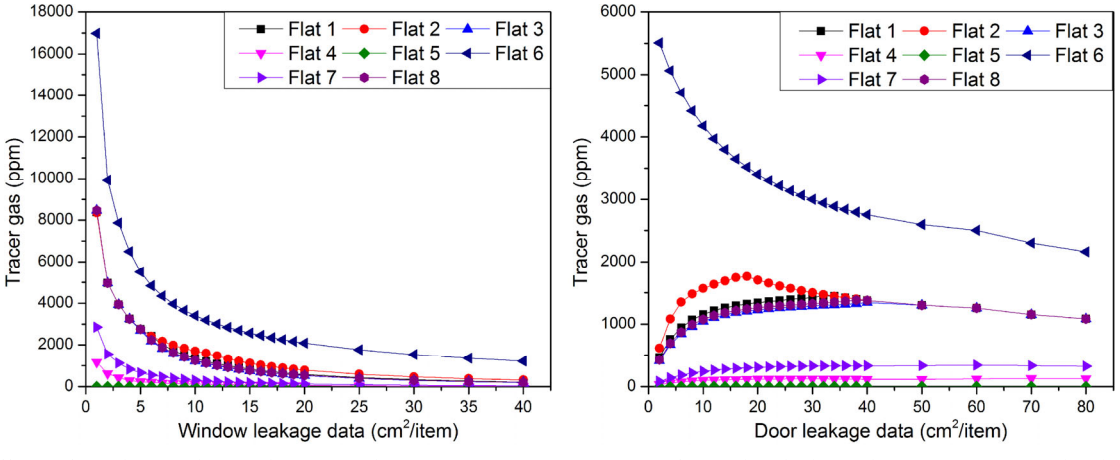

Fig. 13 Effects of window or door tightness on the tracer gas concentration (Left: window leakage change situation, Right: door leakage change situation)

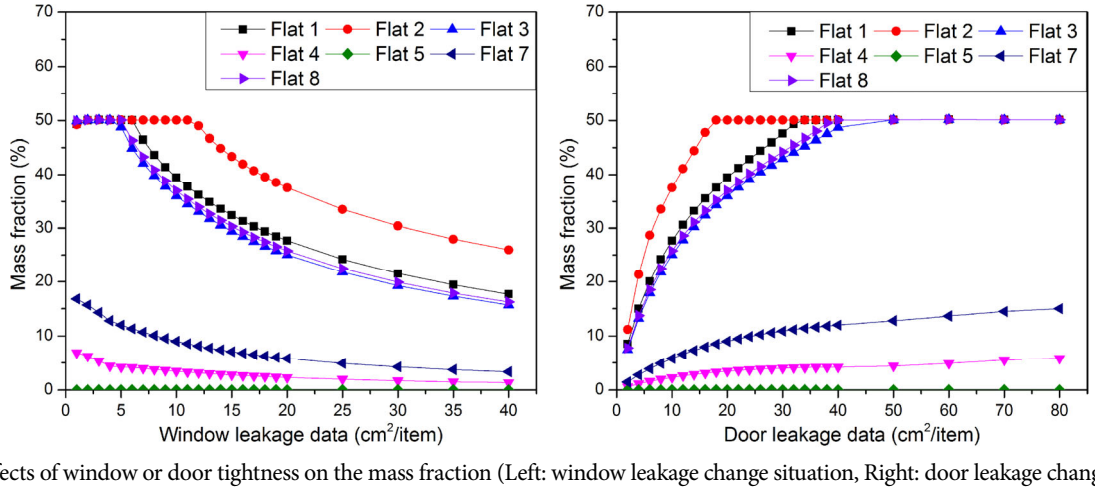

Fig. 14 Effects of window or door tightness on the mass fraction (Left: window leakage change situation, Right: door leakage change situation)

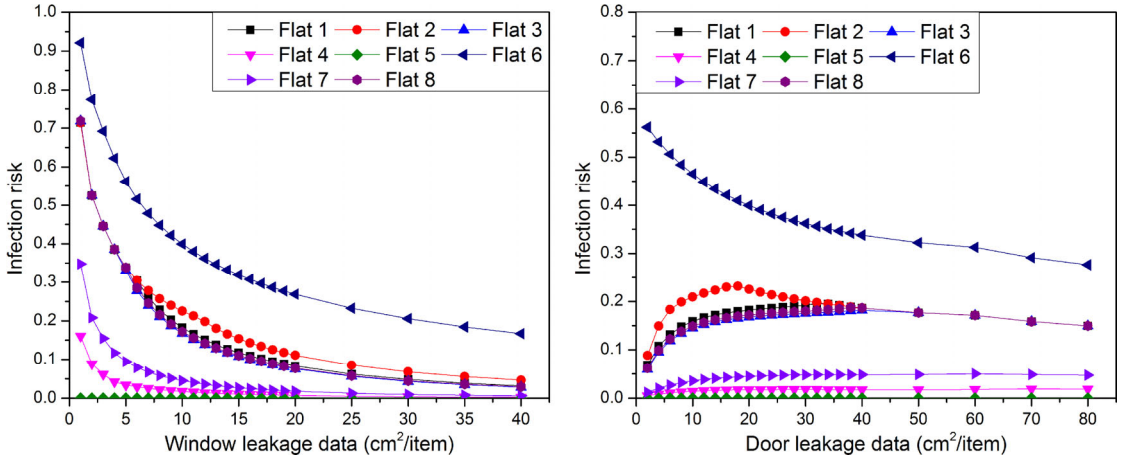

Fig. 15 Effects of window or door tightness on the infectious risk (Left: window leakage change situation, Right: door leakage change situation)

4 Conclusions

The internal inter-unit pollutant dispersion induced by air infiltration was investigated in a HRR building. The pressure coefficients distributions on building façades were obtained from wind tunnel experiments, and the indoor air infiltration and contaminant transmission were calculated using the multi-zone method. The results show that the predicted air infiltration rate is below 0.7 ACH, which is consistent with the recommended value of air leakage under 0.7–0.8 ACH for conserving energy in the ASHRAE handbook. The assessed cross-infection risk can be over 20% because of the low air infiltration rate, which is significantly higher than the risk of 9% obtained in our previous on-site measurement. The inter-unit dispersion induced by air infiltration must not be overlooked. Air infiltration rates increase along building height. This increase is minimal on the leeward side but significant on the windward side. Cross-infection risk between horizontal adjacent units is generally higher on lower floors. The location of the tracer gas source in a unit in relation to the wind direction is determinant on the exposure levels of other units. The presence of a contaminant source in the windward side results in the highest cross-contaminant level to other horizontal adjacent units.

Enlarging external leakage can increase the air change with outdoor fresh air and dilute indoor contaminant, while enlarging internal leakage may enhance inter-unit dispersion. Practically, in the residential building design, internal windows that have potential leakages should be avoided. And the airtightness of individual entrance doors and other doors to public spaces, such as corridors, staircases, and elevators, should be improved. These strategies are also beneficial for the fire control in HHR buildings and meet the privacy requirements for modern living. As far as public health and occupants behaviors are concerned, proper opening external windows should be encouraged, in particular in conjunction with the proper use of mechanical exhausts provided in the bathroom and kitchens. However, these approaches may increase the cross-infection via external routes, such as single-sided natural ventilation. Effective control measures should be further explored considering multiple transmission routes.

Acknowledgements

The research is financially funded by Health and Medical Research Fund, Hong Kong SAR Government, with the project reference no.13121442.

References

Ai ZT, Mak CM (2014). A study of interunit dispersion around multistory buildings with single-sided ventilation under different wind directions. *Atmospheric Environment*, 88: 1–13.

Ai ZT, Mak CM (2016). Large eddy simulation of wind-induced interunit dispersion around multistory buildings. *Indoor Air*, 26: 259–273.

ASHRAE (2007). ASHRAE Handbook—HVAC applications. Atlanta, GA, USA: American Society of Heating, Refrigerating and Air Conditioning Engineers.

Cheng CKC, Lam KM, Leung YTA, Yang K, Li DHW, Cheung SCP (2011). Wind-induced natural ventilation of re-entrant bays in a high-rise building. *Journal of Wind Engineering and Industrial Aerodynamics*, 99: 79–90.

Emmerich SJ (2001). Validation of multizone IAQ modeling of residential-scale buildings: A review. *ASHRAE Transactions*, 107(2): 619–628.

Gao NP, Niu JL, Perino M, Heiselberg P (2008). The airborne transmission of infection between flats in high-rise residential buildings: Tracer gas simulation. *Building and Environment*, 43: 1805–1817.

Gao NP, Niu JL, Perino M, Heiselberg P (2009). The airborne transmission of infection between flats in high-rise residential buildings: Particle simulation. *Building and Environment*, 44: 402–410.

Jomehzadeh F, Nejat P, Calautit JK, Yusof MBM, Zaki SA, Hughes BR, Yazid MNAWM (2016). A review on windcatcher for passive cooling and natural ventilation in buildings, Part 1: Indoor air quality and thermal comfort assessment. *Renewable and Sustainable Energy Reviews*, 70: 736–756.

Karava P, Stathopoulos T, Athienitis AK (2006). Impact of internal pressure coefficients on wind-driven ventilation analysis. *International Journal of Ventilation*, 5: 53–66.

Karava P, Stathopoulos T, Athienitis AK (2007). Wind-induced natural ventilation analysis. *Solar Energy*, 81: 20–30.

Karava P, Stathopoulos T, Athienitis AK (2011). Airflow assessment in cross-ventilated buildings with operable façade elements. *Building and Environment*, 46: 266–279.

Kobayashi T, Sagara K, Yamanaka T, Kotani H, Takeda S, Sandberg M (2009). Stream tube based analysis of problems in prediction of cross-ventilation rate. *International Journal of Ventilation*, 7: 321–334.

Kobayashi T, Sandberg M, Kotani H, Claesson L (2010). Experimental investigation and CFD analysis of cross-ventilated flow through single room detached house model. *Building and Environment*, 45: 2723–2734.

Lai ACK, Nazaroff WW (2000). Modeling indoor particle deposition from turbulent flow onto smooth surfaces. *Journal of Aerosol Science*, 31: 463–476.

Li Y, Delsante A, Symons J (2000). Prediction of natural ventilation in buildings with large openings. *Building and Environment*, 35: 191–206.

Li Y, Duan S, Yu IT, Wong TW (2005). Multi-zone modeling of probable SARS virus transmission by airflow between flats in Block E, Amoy Gardens. *Indoor Air*, 15: 96–111.

Li Y, Leung GM, Tang JW, Yang X, Chao CYH, Lin JZ, Lu JW, Nielsen PV, Niu J, Qian H, et al. (2007). Role of ventilation in airborne transmission of infectious agents in the built environment—A multidisciplinary systematic review. *Indoor Air*, 17: 2–18.

Liu D-L, Nazaroff WW (2003). Particle penetration through building cracks. *Aerosol Science and Technology*, 37: 565–573.

Liu XP (2011). Experimental and numerical investigation of air cross-contamination around typical high-rise residential building in Hong Kong. PhD Thesis, The Hong Kong Polytechnic University.

Liu XP, Niu JL, Kwok KCS, Wang JH, Li BZ (2010). Investigation of indoor air pollutant dispersion and cross-contamination around a typical high-rise residential building: Wind tunnel tests. *Building and Environment*, 45: 1769–1778.

Liu XP, Niu JL, Kwok KC, Wang JH, Li BZ (2011). Local characteristics of cross-unit contamination around high-rise building due to wind effect: Mean concentration and infection risk assessment. *Journal of Hazardous Materials*, 192: 160–167.

Nicas M, Nazaroff WW, Hubbard A (2005). Toward understanding the risk of secondary airborne infection: emission of respirable pathogens. *Journal of Occupational and Environmental Hygiene*, 2: 143–154.

Niu J, Tung TCW (2008). On-site quantification of re-entry ratio of ventilation exhausts in multi-family residential buildings and implications. *Indoor Air*, 18: 12–26.

Nore K, Blocken B, Thue JV (2010). On CFD simulation of wind-induced airflow in narrow ventilated facade cavities: Coupled and decoupled simulations and modelling limitations. *Building and Environment*, 45: 1834–1846.

Parker ST, Lorenzetti DM, Sohn MD (2014). Implementing state-space methods for multizone contaminant transport. *Building and Environment*, 71: 131–139.

Ramponi R, Blocken B (2012). CFD simulation of cross-ventilation for a generic isolated building: Impact of computational parameters. *Building and Environment*, 53: 34–48.

Riley EC, Murphy G, Riley RL (1978). Airborne spread of measles in a suburban elementary school. *American Journal of Epidemiology*, 107: 421–432.

Riley RL (1974). Airborne infection. *The American Journal of Medicine*, 57: 466–475.

Sandberg M (2004). An alternative view on the theory of cross-ventilation. *International Journal of Ventilation*, 2: 409–418.

Seifert J, Li Y, Axley J, Rösler M (2006). Calculation of wind-driven cross ventilation in buildings with large openings. *Journal of Wind Engineering and Industrial Aerodynamics*, 94: 925–947.

Standard ANZ (2011). AS/NZS 1170.2: 2011 Structural Design Actions—Part 2: Wind actions.

Temenos N, Nikolopoulos D, Petraki E, Yannakopoulos PH (2015). Modelling of indoor air quality of Greek apartments using CONTAM (W) software. *Journal of Physical Chemistry & Biophysics*, 5: 190.

Tung TCW, Chao CYH, Burnett J (1999). A methodology to investigate the particulate penetration coefficient through building shell. *Atmospheric Environment*, 33: 881–893.

Walton GN, Dols WS (2003). NISTIR 7251, CONTAM 2.4 User Guide and Program Documentation. Gaithersburg, MD, USA: National Institute of Standards and Technology.

Wang JH, Niu JL, Liu XP, Yu CWF (2010a). Assessment of pollutant dispersion in the re-entrance space of a high-rise residential building, using wind tunnel simulations. *Indoor and Built Environment*, 19: 638–647.

Wang LL, Dols WS, Chen Q (2010b). Using CFD capabilities of CONTAM 3.0 for simulating airflow and contaminant transport in and around buildings. *HVAC&R Research*, 16: 749–763.

Wu Y, Niu J (2016). Assessment of mechanical exhaust in preventing vertical cross-household infections associated with single-sided ventilation. *Building and Environment*, 105: 307–316.

Wu Y, Niu J (2017). Numerical study of inter-building dispersion in residential environments: Prediction methods evaluation and infectious risk assessment. *Building and Environment*, 115: 199–214.

Wu Y, Tung TCW, Niu JL (2016). On-site measurement of tracer gas transmission between horizontal adjacent flats in residential building and cross-infection risk assessment. *Building and Environment*, 99: 13–21.

Yu IT, Li Y, Wong TW, Tam W, Chan AT, Lee JH, Leung DY, Ho T (2004). Evidence of airborne transmission of the severe acute respiratory syndrome virus. *New England Journal of Medicine*, 350: 1731–1739.